






Article

# Evaluating the NO<sub>x</sub> Storage Catalysts (NSC) Aging: A Preliminary Analytical Study with Electronic Microscopy

Leonarda Bellebuono <sup>1</sup>, Cosimo Annese <sup>2</sup>, Lucia Catucci <sup>1</sup> , Giuseppe Colafemmina <sup>1</sup> ,  
Roberto Comparelli <sup>3,\*</sup> , Pietro Cotugno <sup>4</sup>, Francesco Fracassi <sup>1</sup>, Caterina Fusco <sup>2</sup>,  
Angelo Nacci <sup>1,2</sup>  and Lucia D'Accolti <sup>1,2,\*</sup> 

<sup>1</sup> Dipartimento di Chimica, Università di Bari "A. Moro", Via Orabona 4, 70126 Bari, Italy; leonarda.bellebuono@gmail.com (L.B.); lucia.catucci@uniba.it (L.C.); giuseppe.colafemmina@uniba.it (G.C.); francesco.fracassi@uniba.it (F.F.); angelo.nacci@uniba.it (A.N.)

<sup>2</sup> ICCOM-CNR, SS Bari, Via Orabona 4, 70126 Bari, Italy; annese@ba.iccom.cnr.it (C.A.); fusco@ba.iccom.cnr.it (C.F.)

<sup>3</sup> IPCF-CNR, SS Bari, via E. Orabona 4, 70125 Bari, Italy

<sup>4</sup> CONISMA, SS Bari, via E. Orabona 4, 70125 Bari, Italy; pietro.cotugno@uniba.it

\* Correspondence: r.comparelli@ba.ipcf.cnr.it (R.C.); lucia.daccolti@uniba.it (L.D.); Tel.: +39-080-544-2068 (L.D.)

Received: 4 August 2017; Accepted: 12 October 2017; Published: 13 October 2017

**Featured Application:** Could be aided to improve the efficiency of NSC catalysts and thus reduce the environmental impact of thermal-powered vehicles in accordance with the Paris agreement COP21.

**Abstract:** This paper describes an expeditious and reliable method for determining the thermal effects in a static condition of commercial NO<sub>x</sub> storage catalysts (NSCs) using scanning electron microscopy with an energy dispersive X-ray analytical system (SEM/EDS). It is worth remarking that possible changes in the morphology and in the elemental composition of the catalyst may be considered as the most important causes of the lower conversion of NO<sub>x</sub>. The information attained in this work indicates that Pt nanoparticle sintering is strongly increased by the oxygen exposure, and this can be considered a very useful preliminary investigation for the studies already present in the literature on the efficiency of NSCs.

**Keywords:** NO<sub>x</sub> storage catalysts; thermal aging; electronic microscopy

## 1. Introduction

In recent decades, research has focused on the development of catalytic and photocatalytic methods based on the use of nanoparticles (NPs), which can be used in various applications related to chemical production as well as environmental technology. In the latter context, of wide interest is the reduction of greenhouse gases with special focus on the abatement of NO<sub>x</sub> using nanocatalysis [1–3].

The NO<sub>x</sub>s have manifold devastating effects on the atmospheric ecosystem (i.e., ozone layer depletion, acid rain etc.) and on human health. As emerges from several studies, the main contribution to NO<sub>x</sub> emissions comes from automobile sources, with almost half of all NO<sub>x</sub> produced [4].

The NO<sub>x</sub> storage catalyst (NSC) is one of the most promising concepts for the reduction of NO<sub>x</sub> from exhaust gas of lean burn combustion engines such as Diesel engines [5,6]. In the NSC, there are precious metals (platinum, rhodium, palladium), various oxides, and other substances useful for NO<sub>x</sub> storage. The catalytic NSC converter is made of a ceramic (synthetic cordierite 2MgO·2Al<sub>2</sub>O<sub>3</sub>·5SiO<sub>2</sub>) or metallic (chromium-iron-aluminum alloys) monolith, and its internal walls are covered with the

washcoat, a mixture of several oxides such as BaO, ceria, zirconia, and  $\gamma$ -alumina, possessing a high specific area, thus improving the catalytic performances.

The catalytic active phase, composed by one or more noble nanostructured metals, is uniformly dispersed on the washcoat surface and all these components exert a proper role that is based on a complex interaction among themselves [7]. Recent studies have demonstrated that the presence of barium in the washcoat is crucial for the NO<sub>x</sub> storage process, due to the reversible transformation of BaO (or carbonate) into BaNO<sub>3</sub>, and that a great influence is also exerted by cerium [8].

For a Pt–BaO/Al<sub>2</sub>O<sub>3</sub> catalyst, Kim et al. observed that the sintering of platinum particles increases exponentially with both the aging time and the temperature [9], and this not only decreases the conversion of the reactions but also affects the NO<sub>x</sub> storage process [10].

The sintering of both Pt particles and the washcoat phase leads to an inhomogeneous dispersion of the catalytic phase and lowers the number of the active sites for the NO<sub>x</sub> storage [11]. A further drawback of Pt sintering is the decrease in the contact surface between Pt and BaO, resulting not only in a lower activity for the NO oxidation but also in a reduced rate of NO<sub>2</sub> spillover from Pt to the neighboring barium adsorption sites, which in turn decrease the NO<sub>x</sub> storage activity [9–11].

Most of the previous works have shown that the sintering behavior of Pt is a function of time, temperature, and composition of gaseous atmosphere to which the catalyst is exposed [9–12]. However, the sintering dependence on the gaseous environment has commonly been evaluated on model catalysts and has been based on NO<sub>x</sub> conversion efficiency, asserting that the oxidizing atmosphere tends to strongly increase the aging phenomenon [4,12].

Similarly, thermal aging is a serious drawback of today's NSCs, imposing a high regeneration frequency of catalytic material to preserve the high levels of NO<sub>x</sub> conversion.

To the best of our knowledge, few studies have been reported until now on real (commercial) catalysts for automotive applications, such as selective catalytic reduction (SCR) [13], three-way catalysts [14], and NSC catalysts [15,16], aimed at establishing, with quantitative and morphological data, the separate contributions of thermal and chemical (oxidizing) effects to the aging process.

In this context, based on our experience in organocatalysis and nanocatalysis [17–21], we envisaged that these contributions can be evaluated with the aid of electronic microscopy. Herein, we report studies on chemical and structural variations of the Pt particles and the washcoat of commercial NSCs ascertained via TEM and EDS analyses. These investigations can be considered preliminary to the studies already present in the literature on the efficiency of NSCs.

## 2. Materials and Methods

The experiments here were carried out on two commercial monolithic converters presently used on vehicles. One was a ceramic catalyst aged NSC Diesel 2.0 L from which samples were collected by means of stickers coal. The other is a metallic catalytic converter obtained from a prototype application using a Diesel 2000 motor.

The scanning electron microscopy, energy dispersed X-ray, and field emission scanning electron microscopy (FE-SEM) spectra were performed with a Zeiss Sigma microscope operating in the range 0.5–20 kV and equipped with an in-lens secondary electron (SE) detector, a back-scattered electron (BSE) detector, and an INCA Energy Dispersive Spectroscopy (EDS) detector. Samples were deposited on double-sided carbon tape and grounded with silver paste.

Transmission electron microscopy (TEM) analyses were performed with a JEOL JEM-1011 microscope operating at 100 kV. The TEM samples were prepared by casting a drop of powder in CHCl<sub>3</sub> solution onto a carbon hollowed TEM grid.

The BET surface area and pore size of the sorbent were determined by adsorption–desorption N<sub>2</sub> isotherms at 77 K, by an Autosorb IQ Chemi TCD instrument (Quantachrome Instruments, Boynton Beach, FL, USA). The biosorbent was apparently a mesoporous material with pore diameters ranging 20–500 Å, an average pore radius of 16.535 Å, and a BET total surface area exceeding 1.664 m<sup>2</sup>/g. Referring to the pores, the total volume and surface area were, respectively, 0.008 cm<sup>3</sup>/g and 1.010 m<sup>2</sup>/g.

X-ray powder diffraction (PXRD) measurements were carried out with a Panalytical X'PERT PRO powder diffractometer equipped with a mirror and a PIXcel<sup>®</sup> solid state detector in the 20–100° 2 $\theta$  region, operating with Cu K $\alpha$  radiation ( $\lambda = 1.5418 \text{ \AA}$ ). Anti-scatter slits were used both on the incident (0.25° and 0.5° divergence) and the diffracted (7.5 mm height) beam.

**Samples Preparation:** The Diesel 2000 catalyst was cut in slices that were thermally aged in a furnace at 800 °C for 8 and 24 h under an argon atmosphere [5,9,12].

To evaluate the influence of oxygen and water, two samples were subjected to a pretreatment with humid O<sub>2</sub> after which molecular oxygen was flushed in distilled water, and the resulting wet stream was bubbled in a bottle containing the catalyst slices for 2 h at room temperature. Then, the slices were aged for 8 and 24 h respectively. After these treatments, the powdered catalyst, containing the precious metal dispersion, the washcoat, and the alkaline-earth metal oxides were studied with FE-SEM-EDS, TEM, XRD, and BET techniques.

### 3. Results

Investigations began on the ceramic NSC catalyst. A preliminary screening was carried out to find the best technique for revealing morphologic variations of the substrate under the operative conditions.

Firstly, the optical VMS—004D—400x USB Microscope was used to detect deposits on the metal support at the upstream and downstream of the catalytic converter (Figure 1). Deposits, collected by means of stickers coal, were analyzed via scanning electron microscopy—energy dispersed X-ray (SEM-EDS) techniques.

Analyses of the upstream sample revealed the presence of magnesium, silicon, and aluminum, constituents of the ceramic monolith (Figure 2B).

As expected, barium and cerium (as oxides) were also detected, which were added to improve the catalytic activity. The aluminum peak was due not only to the  $\gamma$ -alumina but also to the aluminum of the ceramic monolith. Since the exhaust gas entering the converter contains sulfur, the latter was also detected in the upstream sample.

EDS analyses of the downstream sample revealed the absence of both sulfur and platinum elements (Figure 2D). In the case of the former, this was not a surprising result, because the ceramic monolith is expected to purify the exhaust gas from SO<sub>x</sub> compounds efficiently. In contrast, the lack of platinum in the downstream sample is an unexpected novelty and can be seen as a choice of the manufacturer, who decided that the presence of Pt in that section of device was an unnecessary cost, since much of the conversion process (including NO<sub>x</sub> reduction to N<sub>2</sub>) takes place at the start of converter.

In contrast, SEM images provide only rough morphological information that is not sufficient to point out differences between the two samples (Figure 2A,C).

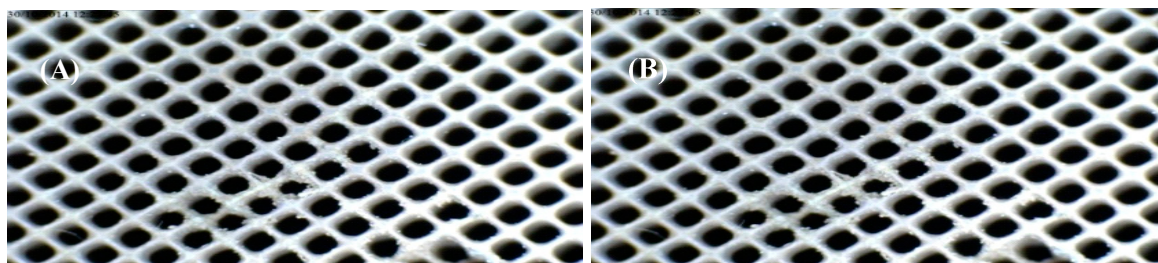
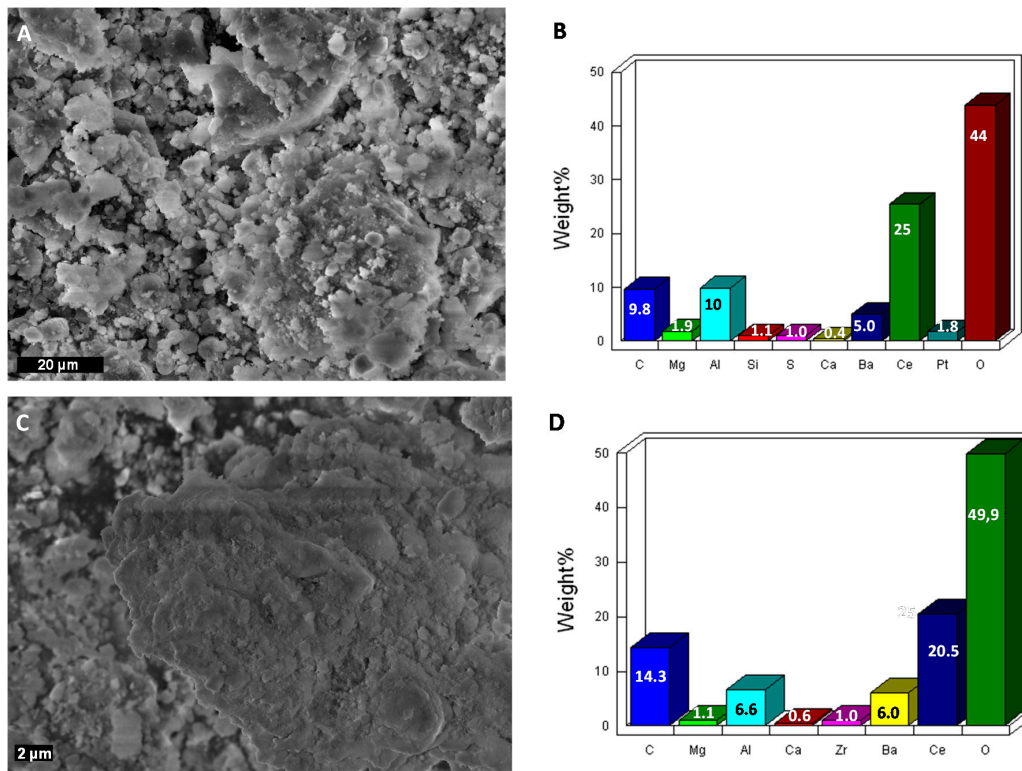
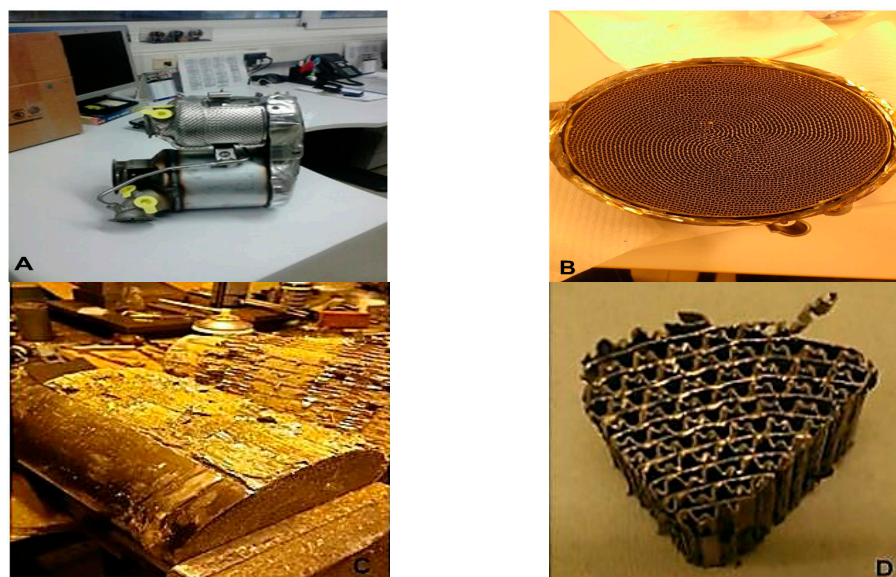


Figure 1. (A) Upstream and (B) downstream samples of the ceramic support.



**Figure 2.** NSC ceramic support: (A) SEM image and (B) EDS analysis of the upstream sample; (C) SEM image and (D) EDS analysis of the downstream sample.

Next, we turned our attention to the metallic catalytic converter, Diesel 2000 (Figure 3). In this case, sampling was carried out in a careful manner in order to obtain uniform and representative specimens, after which chemical composition throughout the catalyst was preliminarily investigated by EDS analyses, sampling both the upstream and downstream parts of NSC catalyst (Figure 4).



**Figure 3.** NSC metallic catalytic converter: (A) the whole catalyst; (B) the metallic support; (C) longitudinal cuts; (D) a slice of the catalyst.

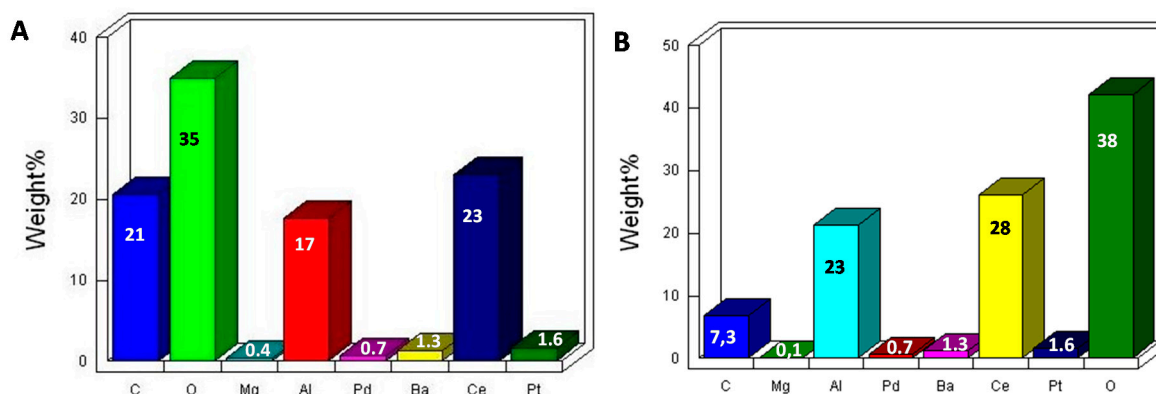


**Figure 4.** EDS analysis of the (A) upstream and (B) downstream samples of the NSC metallic catalysts.

As EDS quantitative data showed a roughly uniform elemental composition along the entire NSC, with the exception of carbon percentage, which depends on sampling, specimens were obtained by cutting the catalyst first longitudinally (Figure 3C) and then transversally to produce slices among which the ones with unblocked pores were chosen (Figure 3D).

Recent studies showed that some compounds in the exhaust feed can influence the NO<sub>x</sub> storage process, especially CO<sub>2</sub> and water vapor, since these substances can be easily adsorbed on barium and alumina sites and can sterically block their active sites [10–12]. Therefore, when water vapor is present in the exhaust gas, the storage capacity of NO<sub>x</sub> on NSC is expected to be reduced.

On these bases, with the aim of evaluating separately the contributions to the aging of the thermal treatment and the gaseous environment exposure, the samples listed in Table 1 were prepared, in which some slices of the catalyst were subjected to heating under argon atmosphere (namely NSC\_8\_Ar and NSC\_24\_Ar), to assess the sole thermal effect, while other ones were exposed, under the same thermic conditions, to a humid oxygen atmosphere (namely NSC\_8\_O<sub>2</sub> and NSC\_24\_O<sub>2</sub>) to evaluate the influence of a chemical oxidizing gaseous environment [7,9–12] at 800 °C, which is higher than the maximum temperature used for NSC catalysts.

**Table 1.** Thermal aging tests of NSC slices <sup>1</sup>.

SAMPLE	T (800 °C)	Wet O <sub>2</sub> Pretreatment	Time (h)
NSC_8_Ar	DONE	NONE	8
NSC_24_Ar	DONE	NONE	24
NSC_8_O <sub>2</sub>	DONE	DONE	8
NSC_24_O <sub>2</sub>	DONE	DONE	24

<sup>1</sup> Operating conditions as reported into the experimental section.

All samples were subjected to SEM-EDS and TEM analyses and compared with those of the pristine material. Concerning the SEM-EDS analyses, only the sample coming from the thermic treatment under a humid oxygen atmosphere (sample NSC\_24\_O<sub>2</sub>) somehow displayed different results with respect to the pristine material. Indeed, from the EDS analyses of both samples, reported in Figure 5B, the presence of the expected elemental components of an NSC, namely Al, Ba, Ce, and Pt, was found, but the other precious metal Pd was not present in relevant amounts. As expected, after the thermal aging process was carried out for 24 h at 800 °C under O<sub>2</sub> exposure, the oxygen peak remarkably increased the intensity, a predictable phenomenon that can be explained both by the formation of several oxides and by the adsorption of molecular oxygen on the active sites (Figure 5D).

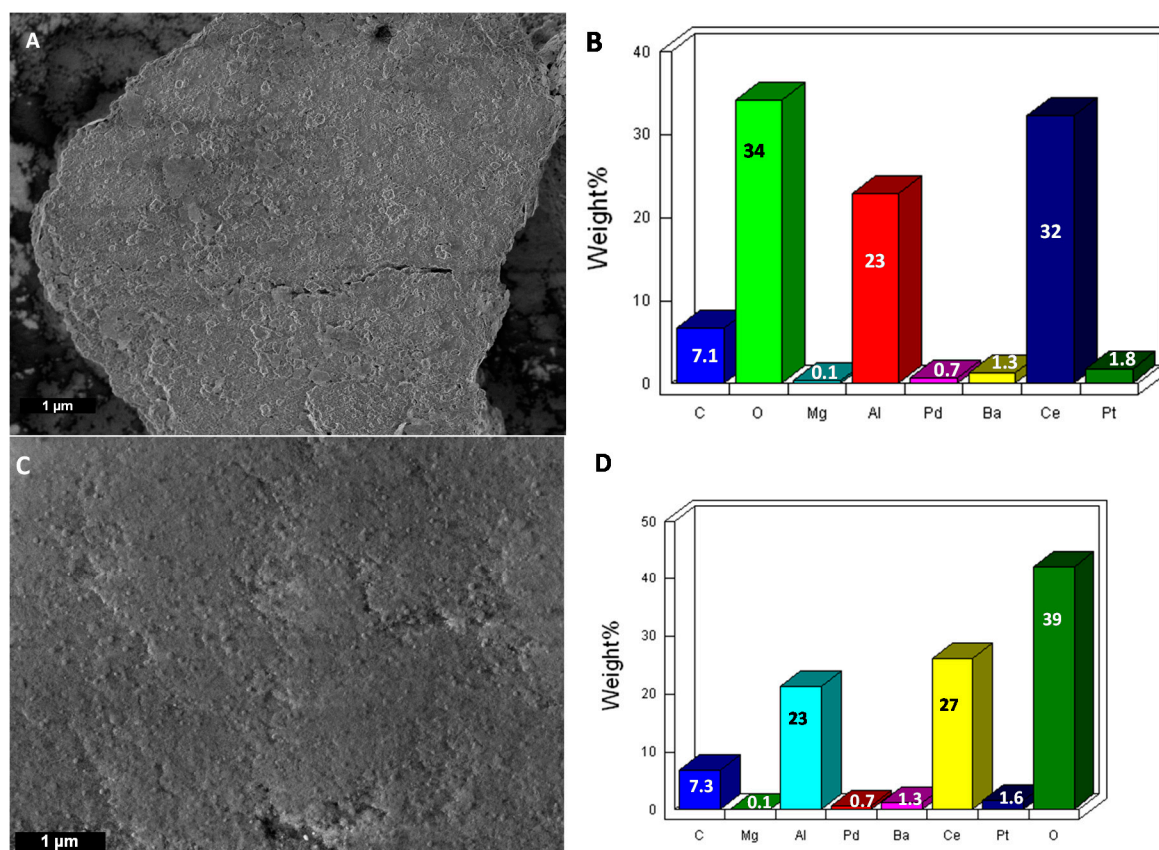


**Figure 5.** (A) SEM image and (B) EDS analysis of a pristine sample of NSC catalyst; (C) SEM image and (D) EDS analysis of NSC\_24h\_O<sub>2</sub>.

Similar to the case of ceramic catalysts, a comparison of the SEM images of pristine and thermally aged catalysts was not sufficient in terms of evaluating the entity of the aging process (Figure 5A,C). In contrast, the TEM technique proved to be much more effective in investigating the catalyst evolution, enabling the determination of the nanostructured Pt particle size distribution, a crucial parameter for establishing the NSC catalyst functioning.

In fact, it is well known that a primary role of Pt in the NO<sub>x</sub> abatement process is the oxidation NO → NO<sub>2</sub>, which is also the first step of the NO<sub>x</sub> storage process. In addition, the proposed mechanism for storage invokes a reversible surface spillover step of NO<sub>2</sub> occurring between Pt and BaO sites. Therefore, to maintain a uniform distribution of Pt nanoparticles into the BaO matrix avoiding the sintering phenomenon is of crucial importance for achieving high rates of both NO<sub>x</sub> storage and its release [22]. A possible way to avoid Pt sintering is the control of the temperature, which should be maintained as low as possible (ideally lower than 600 °C), particularly when an oxidizing atmosphere is present [9].

To gain experimental evidence of these facts, TEM analyses were conducted on samples listed in Table 1, focusing attention on the Pt nanoparticle size evolution (Figure 6). TEM images, corroborated by statistical analyses (Table 2), pointed out remarkable modifications with respect to the pristine sample of Pt nanoparticle morphology and sizes after thermal treatment, particularly after prolonged exposure to oxygen.

Indeed, while the Pt nanoparticles (dark spots in Figure 6) of samples NSC\_8\_O<sub>2</sub> and NSC\_24\_Ar, experienced only a slight increase in size, the sample heated for 24 h and exposed to a humid oxygen atmosphere (NSC\_24\_O<sub>2</sub>) underwent a dramatic growth of particles (Figure 6D).

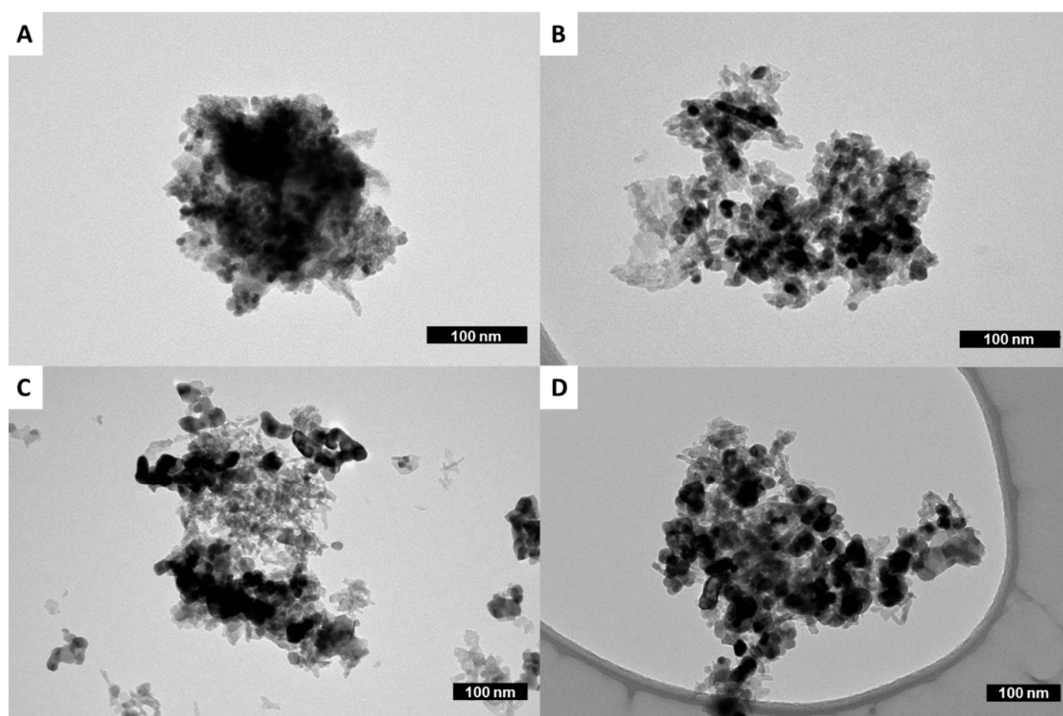


**Figure 6.** TEM images of (A) the pristine NSC catalyst and of samples (B) NSC\_8\_O<sub>2</sub>, (C) NSC\_24\_Ar, and (D) NSC\_24\_O<sub>2</sub>.

Data reported in Table 2 highlight the growth of Pt nanoparticles from 8 to 43 nm as well as the broadening of their sizes distribution from 12 to 20%. These data clearly demonstrate that the sintering process is strongly accelerated by the oxidizing gaseous environments, with an increment of Pt particle sizes of more than 5 times in only 24 h of exposure.

**Table 2.** Pt NP size distribution  $\pm$  standard deviation as a function of thermal treatment duration and oxygen exposure.

SAMPLE	Size (nm)
Pristine	8 $\pm$ 1
NSC_8_Ar	11 $\pm$ 2
NSC_8_O <sub>2</sub>	12 $\pm$ 3
NSC_24_Ar	15 $\pm$ 5
NSC_24_O <sub>2</sub>	43 $\pm$ 9

As catalytic performances of these NSC catalysts are also strongly dependent on structural factors of the washcoat, such as its crystal lattice and specific surface area, BET and XRD analyses were carried in order to highlight possible variations of this part of the catalyst induced by thermal treatment and oxygen exposure.

From data in Table 3, it can be clearly seen that the specific surface area of the washcoat, including the pore diameter and the volume, does not undergo significant variations with treatment.

**Table 3.** BET analyses.

Sample	Pores Diameter (Å)	Pores Volume (cm <sup>3</sup> /g)	BET Area (m <sup>2</sup> /g)
Pristine	37.0	0.5	1012
NSC_24_Ar	40.8	0.4	994
NSC_24_O <sub>2</sub>	44.1	0.3	98

Similar conclusions can be drawn on the basis of XRD analyses (Figure 7), for which the crystalline structure of the major oxide components of the washcoat (BaO,  $\gamma$ -alumina, and ceria) does not undergo substantial changes after the treatments. It should be noted that the XRD spectrum seems to be useless for this purpose because of the widening of peaks due to the contributions of the various oxides that drop to 2theta values that are very close to each other. In addition, due to the small percentages, platinum peaks are not useful for speculating on possible variations in the structure. Therefore, the real changes detected are due to the sintering of platinum nanoparticles, which is well evidenced by TEM analyses of Figure 6.

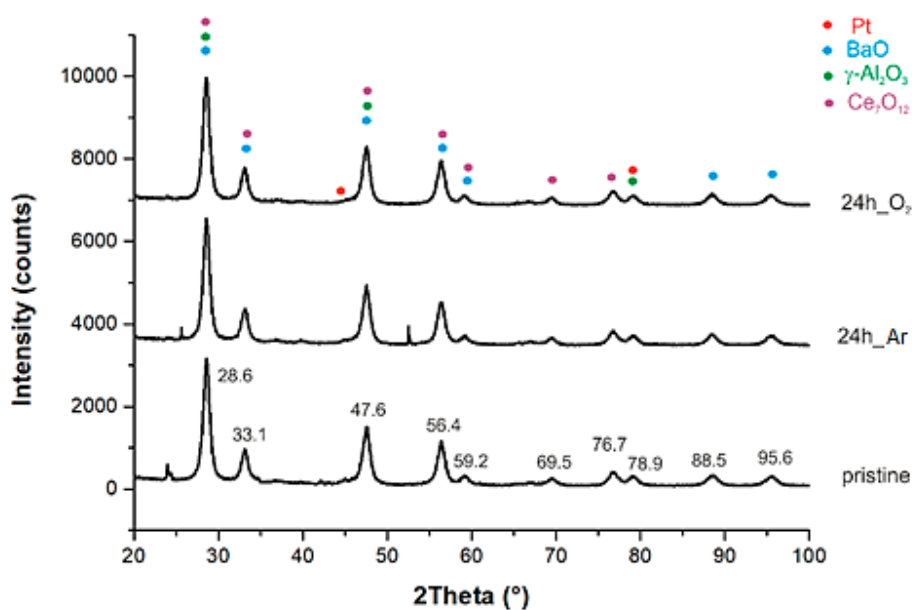


**Figure 7.** XRD analyses of NSC samples. Colored points indicate the overlap of peaks due to the different oxides assigned based on the literature [23–27].

In conclusion, we have demonstrated that NSC aging can be studied carefully by means of electronic microscopy (SEM-EDS and TEM techniques) evaluating for the first time on real (commercial) samples the separate effects of thermal and chemical (oxidizing environment) treatment. Besides morphology and size distribution, EDS analyses provide chemical compositions of the catalyst environment, and all these data can provide a precise snapshot of the catalyst life. It should be noted that alternative methods exist, such as the traditional basic I/M (idle) tests or the borescope technique developed by Olympus of America, but these techniques do not yield as accurate a diagnosis of the health state of the catalyst [28]. The information attained with these techniques allowed for the direct observation that Pt nanoparticle sintering is strongly increased by oxygen exposure.

This can be considered a very useful preliminary investigation for the studies already present in the literature on the efficiency of NSCs, as it clearly demonstrates, based on quantitative data, that an increased resistance of NSCs to thermal aging is possible if the presence of moisture and oxygen into the exhaust gases is reduced.

**Acknowledgments:** Thanks to Centro Studi Componenti per Veicoli S.p.A. Società Unipersonale del gruppo BOSCH, Modugno (BA), Zona Industriale, Via delle Ortensie, 19 for financial support. Thanks are due to Dott. Ing. Maria Rosaria Gaballo for helpful discussions.

**Author Contributions:** L.B. and C.A. performed the experiments, P.C. and G.C. performed the preparation of Metallic sample, R.C. and F.F. performed the SEM EDS analysis; R.C. performed TEM analysis, C.F., L.C., and A.N. performed preliminary analysis on the ceramic NSC catalyst and analyzed the data on the metallic sample. L.D. conceived and designed the experiments L.D., and A.N. wrote the paper.

**Conflicts of Interest:** The authors declare no conflict of interest.



## References and Note

1. Gawande, M.B.; Goswami, A.; Felpin, F.-X.; Asefa, T.; Huang, X.; Silva, R.; Zou, X.; Zboril, R.; Varma, R.S. Cu and Cu-Based Nanoparticles: Synthesis and Applications in Catalysis. *Chem. Rev.* **2016**, *116*, 3722–3811. [[CrossRef](#)] [[PubMed](#)]
2. Maeda, K.; Domen, K. Development of Novel Photocatalyst and Cocatalyst Materials for Water Splitting under Visible Light. *Bull. Chem. Soc. Jpn.* **2016**, *89*, 627–648. [[CrossRef](#)]
3. Abe, H.; Liu, J.; Ariga, K. Catalytic nanoarchitectonics for environmentally compatible energy generation. *Mater. Today* **2016**, *19*, 12–18. [[CrossRef](#)]
4. Roy, S.; Baiker, A. NO<sub>x</sub> Storage-reduction catalysis: From mechanism and materials properties to storage-reduction performance. *Chem. Rev.* **2009**, *109*, 4054–4091. [[CrossRef](#)] [[PubMed](#)]
5. Epling, W.S.; Campbell, L.E.; Yezerets, A.; Currier, N.W.; Parks, J.E. Overview of the fundamental reactions and degradation mechanisms of NO<sub>x</sub> storage/reduction catalysts. *Cat. Rev.* **2004**, *46*, 163–245. [[CrossRef](#)]
6. Schmeißer, V.; Perez, J.; Tuttlies, U.; Eigenberger, G. Experimental results concerning the role of Pt, Rh, Ba, Ce and Al<sub>2</sub>O<sub>3</sub> on NO<sub>x</sub>-storage catalyst behaviour. *Top. Catal.* **2007**, *42–43*, 15–19. [[CrossRef](#)]
7. Boll, W.; Tischer, S.; Deutschmann, O. Loading and Aging Effects in Exhaust Gas After-Treatment Catalysts with Pt As Active Component. *Ind. Eng. Chem. Res.* **2010**, *49*, 10303–10310. [[CrossRef](#)]
8. Wang, P.; Yi, J.; Gu, W.; Luo, P.; Lei, L. The influence of xMnyCe/c-Al<sub>2</sub>O<sub>3</sub> on NO<sub>x</sub> catalysts on the properties of NO<sub>x</sub> storage and reduction over Pt-Ce-Ba/c-Al<sub>2</sub>O<sub>3</sub> catalysts. *Chem. Eng. J.* **2017**, *325*, 700–707. [[CrossRef](#)]
9. Kim, D.; Chin, Y.; Muntean, G.; Yezeretz, A.; Currier, N.; Epling, W.; Chen, H.; Hess, H.; Peden, C. Relationship of Pt Particle Size to the NO<sub>x</sub> Storage Performance of Thermally Aged Pt/BaO/Al<sub>2</sub>O<sub>3</sub> Lean NO<sub>x</sub> Trap Catalysts. *Ind. Eng. Chem. Res.* **2006**, *45*, 8815–8821. [[CrossRef](#)]
10. Hauff, K.; Tuttlies, U.; Eigenberg, G.; Nieken, U. Reaction Kinetics of Aged NO<sub>x</sub> Storage Catalysts. *Ind. Eng. Chem. Res.* **2013**, *53*, 8399–8409. [[CrossRef](#)]
11. Ji, Y.; Easterling, V.; Graham, U.; Fisk, C.; Crocker, M.; Choi, J.-S. Effect of aging on the NO<sub>x</sub> storage and regeneration characteristics of fully formulated lean NO<sub>x</sub> trap catalysts. *Appl. Catal. B* **2011**, *103*, 413–427. [[CrossRef](#)]
12. Olsson, L.; Fridell, E. The Influence of Pt Oxide Formation and Pt Dispersion on the Reactions NO<sub>2</sub> ⇌ NO + 1/2 O<sub>2</sub> over Pt/Al<sub>2</sub>O<sub>3</sub> and Pt/BaO/Al<sub>2</sub>O<sub>3</sub>. *J. Catal.* **2002**, *210*, 340–353. [[CrossRef](#)]
13. Millo, F.; Rafigh, M.; Fino, D.; Miceli, P. Application of a global kinetic model on an SCR coated on Filter (SCR-F) catalyst for automotive applications. *Fuel* **2017**, *198*, 183–192. [[CrossRef](#)]
14. Fathali, A.; Olsson, L.; Ekström, F.; Laurell, M.; Andersson, B. Hydrothermal Aging-Induced Changes in Washcoats of Commercial Three-Way Catalysts. *Top. Catal.* **2013**, *56*, 323–328. [[CrossRef](#)]
15. De Abreu, G.J.E.; Olsson, L.; Malin, B.; Kristoffersson, A.; Gustafson, L.; Hicks, M. Performance Studies and Correlation between Vehicle- and Rapid- Aged Commercial Lean NO<sub>x</sub> Trap Catalysts. *SAE Int. J. Eng.* **2017**, *10*. [[CrossRef](#)]
16. Myung, C.-L.; Jang, W.; Kwon, S.; Ko, J.; Jin, D.; Park, S. Evaluation of the realtime de-NO<sub>x</sub> performance characteristics of a LNT-equipped Euro-6 diesel passenger car with various vehicle emissions certification cycles. *Energy* **2017**, *132*, 356–369. [[CrossRef](#)]
17. Casiello, M.; Iannone, F.; Cotugno, P.; Monopoli, A.; Cioffi, N.; Ciminale, F.; Trzeciak, A.M.; Nacci, A. Copper(II)-catalysed oxidative carbonylation of aminols and amines in water: A direct access to oxazolidinones, ureas and carbamates. *J. Mol. Catal. A* **2015**, *407*, 8–14. [[CrossRef](#)]
18. D'Accolti, L.; Fiorentino, M.; Fusco, C.; Capitelli, F.; Curci, R. Stereoselective dioxirane hydroxylations and the synthesis of tripod boronic acid esters. *TeLe* **2007**, *48*, 3575–3578. [[CrossRef](#)]
19. Annese, C.; D'Accolti, L.; Fusco, C.; Licini, G.; Zonta, C. Heterolytic (2 e) vs. Homolytic (1 e) Oxidation Reactivity: N–H versus C–H Switch in the Oxidation of Lactams by Dioxirans. *Chem. Eur. J.* **2017**, *23*, 259–262. [[CrossRef](#)] [[PubMed](#)]
20. Ventrella, A.; Catucci, L.; Agostiano, A. Herbicides affect fluorescence and electron transfer activity of spinach chloroplasts, thylakoid membranes and isolated Photosystem II. *Bioelectrochemistry* **2010**, *79*, 43–49. [[CrossRef](#)] [[PubMed](#)]
21. Dilonardo, E.; Milella, A.; Palumbo, F.; Thery, J.; Martin, S.; Barucca, G.; Mengucci, P.; D'Agostino, R.; Fracassi, F. Plasma deposited Pt-containing hydrocarbon thin films as electrocatalysts for PEM fuel cell. *J. Mater. Chem.* **2010**, *20*, 10224–10227. [[CrossRef](#)]

22. Desokumastuti, A.; Staudt, T.; Qin, Z.; Happel, M.; Laurin, M.; Lykhach, Y.; Shaikutdinov, S.; Rohr, F.; Libuda, J. Interaction of NO<sub>2</sub> with model NSR catalysts: Metal-oxide interaction controls initial NO<sub>x</sub> storage mechanism. *Chem. Phys. Chem.* **2008**, *9*, 2191–2197. [[CrossRef](#)] [[PubMed](#)]
23. Santos, A.C.S.F.; Damyanova, S.; Teixeira, G.N.R.; Mattos, L.V.; Noronha, F.B.; Passos, F.B.; Bueno, J.M.C. The effect of ceria content on the performance of Pt/CeO<sub>2</sub>/Al<sub>2</sub>O<sub>3</sub> catalysts in the partial oxidation of methane. *Appl. Catal. A* **2005**, *290*, 123–132. [[CrossRef](#)]
24. Kahler, H. The Crystalline Structures of Sputtered AndEvaporated Metallic Films. *Phys. Rev.* **1921**, *18*, 210–216. [[CrossRef](#)]
25. Gerlach, W. Izvestiya Akademii Nauk SSSR. *Seryia Fizicheskaya* **1956**, *20*, 1105.
26. McAtee, J.L.; Milligan, W.O. Flow Properties of Alumisum Dilatirate-Toluene Gels. *J. Phys. Chem.* **1956**, *60*, 273.
27. Cox, D.E.; Ray, S.P. X-Ray and Neutron Diffraction Study of Intermediate Phasesin Nonstoichiometric Cerium Dioxide. *J. Solid State Chem.* **1975**, *15*, 344.
28. The borescope technique is based on a optic fiber device which can be inserted in an oxygen sensor hole (or other openings) and maneuvered through the exhaust system up to the catalyst. In this case it is possible to only a visual check, without being able to define it morphology, nor the chemical composition of the catalytic converter.



© 2017 by the authors. Licensee MDPI, Basel, Switzerland. This article is an open access article distributed under the terms and conditions of the Creative Commons Attribution (CC BY) license (<http://creativecommons.org/licenses/by/4.0/>).